Manuscript prepared for Atmos. Chem. Phys.
with version 4.3 of the LaTeX class copernicus.cls.
Date: 6 June 2014

The fate of NO_x emissions due to nocturnal oxidation at high latitudes: 1-D simulations and sensitivity experiments

P. L. Joyce[1,2], R. von Glasow[3], and W. R. Simpson[1,2]

[1]Department of Chemistry and Biochemistry, University of Alaska, Fairbanks, AK, USA
[2]Geophysical Institute, University of Alaska, Fairbanks, AK, USA
[3]Centre for Ocean and Atmospheric Sciences, School of Environmental Sciences, University of East Anglia, Norwich, UK

Correspondence to: W. R. Simpson (wrsimpson@alaska.edu) and R. von Glasow (r.von-Glasow@uea.ac.uk)

Abstract.

The fate of nitrogen oxide pollution during high-latitude winter is controlled by reactions of dinitrogen pentoxide (N_2O_5) and is highly affected by the competition between heterogeneous atmospheric reactions and deposition to the snowpack. MISTRA, a 1-D photochemical model, simulated an urban pollution plume from Fairbanks, Alaska to investigate this competition of N_2O_5 reactions and explore sensitivity to model parameters. It was found that dry deposition of N_2O_5 made up a significant fraction of N_2O_5 loss near the snowpack, but reactions on aerosol particles dominated loss of N_2O_5 over the integrated atmospheric column. Sensitivity experiments found the fate of NO_x emissions were most sensitive to NO emission flux, photolysis rates, and ambient temperature. The results indicate a strong sensitivity to urban area density, season and clouds, and temperature, implying a strong sensitivity of the results to urban planning and climate change. Results suggest that secondary formation of particulate ($PM_{2.5}$) nitrate in the Fairbanks downtown area does not contribute significant mass to the total $PM_{2.5}$ concentration, but appreciable amounts are formed downwind of downtown due to nocturnal NO_x oxidation and subsequent reaction with ammonia on aerosol particles.

1 Introduction

The high-latitude winter is a unique chemical environment characterized by extreme cold, extended periods of darkness, and constant snow cover. As the world's population increases, high latitudes are likely to see increased population, enhanced urbanization, and increased resource extraction, all leading to increased pollution emissions including nitrogen-containing species. Anthropogenic nitric

oxide (NO) emissions react to form nitrogen dioxide (NO_2), and together they form the chemical family of NO_x, which is ultimately removed through further oxidation to form nitric acid (HNO_3). Nitric acid can acidify aerosol particles in the atmosphere or deposit to the ground where it has been found to affect ecosystems adversely (Fenn et al., 2003). In sunlit conditions, the principal removal pathway of NO_2 is reaction with OH (Seinfeld and Pandis, 2006) and this reaction can form significant amounts of HNO_3 during the day, particularly in polluted regions (Finlayson-Pitts and Pitts, 2000). In the absence of photolysis, the "dark" reaction pathway forms the intermediate species nitrate radical (NO_3) and dinitrogen pentoxide (N_2O_5), which have both been measured in the nocturnal boundary layer (e.g. Brown et al., 2003; Wood et al., 2005; Ayers and Simpson, 2006; Osthoff et al., 2008; Chang et al., 2011; Riedel et al., 2012; Wagner et al., 2013). The dark reaction pathway includes Reactions (R1) to (R3), followed by either Reaction (R4a) or (R4b):

$$NO + O_3 \rightarrow NO_2 + O_2 \quad \text{(R1)}$$

$$NO_2 + O_3 \rightarrow NO_3 + O_2 \quad \text{(R2)}$$

$$NO_2 + NO_3 \rightleftharpoons N_2O_5 \quad \text{(R3)}$$

$$N_2O_5 + H_2O \xrightarrow{surface} 2HNO_3 \quad \text{(R4a)}$$

$$N_2O_5 + Cl^- \xrightarrow{surface} ClNO_2 + NO_3^- \quad \text{(R4b)}$$

The absence of photolysis allows NO_3 to exist in sufficient concentration for Reaction (R3) to occur and cold temperatures hinder the dissociation of N_2O_5, making the cold and dark conditions of high-latitude winter ideal for N_2O_5 formation. Upon formation, N_2O_5 can undergo heterogeneous hydrolysis through Reaction (R4a) on the surface of an aerosol particle in the atmosphere or the snowpack surface on the ground to form HNO_3. Alternatively, N_2O_5 can react with Cl^- (Reaction R4b) after uptake in an aerosol particle to form nitryl chloride ($ClNO_2$), which is volatile and quickly enters the gas phase. Figure 1 outlines the dark oxidation pathway reaction sequence and the competing removal of N_2O_5 by reactions on aerosol particles and the snowpack. Cold and dark conditions of high-latitude winter encourage loss of NO_x via the dark oxidation pathway. In a modeling study, Dentener and Crutzen (1993) found that 80 % of high latitude NO_x is lost through the dark oxidation pathway in winter. Measurements by Wood et al. (2005) at mid latitudes found total HNO_3 produced by N_2O_5 hydrolysis during the night can be comparable to ambient NO_2 concentrations, suggesting total HNO_3 produced by heterogeneous hydrolysis may be greater at high latitudes during winter.

The probability of a heterogeneous reaction of N_2O_5 to occur upon a molecular collision with an aerosol particle surface is described through the reactive uptake coefficient, γ. Laboratory and field studies have shown γ can be affected by aerosol particle chemical composition (Hanson and Ravishankara, 1991; Van Doren et al., 1991; Chang et al., 2011; Gaston et al., 2013). In a mid-latitude

flight campaign, Brown et al. (2007a) observed a strong dependence of γ on particle acidity and composition. Laboratory analysis has found high concentrations of NO_3^- in aerosol particles can hinder uptake of N_2O_5 and suppress γ in a phenomena known as the "nitrate effect" (Mentel et al., 1999). Additionally, Reaction (R4b) was presented by Graedel and Keene (1995) as a sink of N_2O_5 and the product, $ClNO_2$, has been observed in the atmosphere (Osthoff et al., 2008; Thornton et al., 2010). Bertram and Thornton (2009) found trace amounts of Cl^-, when the molar $Cl^-/NO_3^- > 0.1$, can negate the nitrate effect. They have characterized γ's dependence on aerosol liquid water content, aqueous Cl^- concentration, and aqueous NO_3^- concentration in a parameterization for mixed organic and inorganic aerosol particles in the laboratory.

Other methods for parameterizing gamma have been developed. Chang et al. (2011) wrote an excellent review article on N_2O_5 heterogeneous hydrolysis that describes various models for γ, comparison to ambient measurements, and size and chemical composition effects on γ. The nitrate effect and production of nitryl chloride are well documented by Chang et al. (2011) and cited references, as well as the effect of organic aerosol particle components, which generally is indicated to reduce γ, as described below. Evans and Jacob (2005) parameterized γ based upon aerosol particle type, and for some types γ was a function of temperature and relative humidity and performed global model simulations resulting in a global mean $\gamma = 0.02$, which is lower than Dentener and Crutzen (1993), but often larger than predicted by Bertram and Thornton (2009)'s model. Anttila et al. (2006) described a resistor model for how organic coatings on inorganic core / organic shell aerosol particles could slow heterogeneous hydrolysis and Riemer et al. (2009) found that inclusion of these coatings slowed nitrate formation in a modeling study. Gaston et al. (2013) performed laboratory studies of the reduction of γ due to addition of organic to ammonium bisulfate aerosol particles. They found that low O:C ratio (atomic O:C ratio < 0.5) suppressed γ, while more highly oxygenated (O:C ratio > 0.8) species had little effect on γ. Ambient observations of γ (Bertram et al., 2009; Riedel et al., 2012; Ryder et al., 2014) or modeling of ambient levels of N_2O_5 where γ is varied in the model to constrain its value (Brown et al., 2009; Wagner et al., 2013) have generally found that field measured γ values are lower by factors of 2 or more than the Bertram and Thornton (2009) parameterization. More recent studies have indicated that the inclusion of organic aerosol information and particle mixing state improved the agreement between modeled and observed γ, but overprediction by ~ 2 times still exists in polluted airmasses (Ryder et al., 2014). Only one study of γ during wintertime has been reported upon by Wagner et al. (2013). This study supports the nitrate effect, but unlike the other studies finds that the wintertime observed γ can be larger than that of the Bertram and Thornton (2009) model.

Because pollution is typically emitted at or near ground level, vertical gradients of reactive nitrogen species can easily form in nocturnal boundary layers, especially in cold and stable conditions. Observations of vertical distributions of NO_3 and N_2O_5 demonstrated that nocturnal mixing ratios can vary widely over vertical scales of $10\,\mathrm{m}$ or less, implying that NO_3 and N_2O_5 occupy distinctly

different chemical regimes as a function of altitude (Brown et al., 2007b; Wagner et al., 2013). Aircraft observations of NO_3 and N_2O_5 show that these species occur at larger concentrations and are longer lived aloft than they are near the ground (Brown et al., 2007a). A modeling study by Geyer and Stutz (2004) found that slow upward transport of NO emitted near the ground, and the simultaneously occurring chemistry, controlled the vertical structure of the chemistry of NO_x, NO_3, and N_2O_5.

Such observations of vertical gradients of nocturnal nitrogen species may be due to competition between the removal of N_2O_5 through Reaction (R4a) or (R4b) on aerosol particle surfaces aloft vs. deposition to the ground. Measurements of N_2O_5 near Fairbanks in winter by our group found sinks of N_2O_5 (presumably heterogeneous chemistry) were an efficient mechanism for NO_x removal near ground level (Ayers and Simpson, 2006). Apodaca et al. (2008) found that dry aerosol surface area was insufficient to explain the loss of N_2O_5 observed, suggesting loss to other surfaces plays a key role. To characterize loss to the snowpack, Huff et al. (2011) found the deposition velocity of N_2O_5 to be $0.59 \pm 0.47\,\mathrm{cm\,s^{-1}}$ and that dry deposition represents at least $1/8$ of the total chemical removal of N_2O_5 near the ground. Theoretical studies of Kramm et al. (1995) calculated a somewhat higher N_2O_5 deposition velocity that is towards the high end of our sensitivity studies. Understanding the magnitude of relative loss rates is essential for interpretation of N_2O_5 measurements performed at ground level since air parcels near the ground surface will undergo both loss to aerosol particles and the snowpack.

Here we use a 1-D atmospheric chemistry model to address the fate of emitted NO_x in high-latitude winter. A 1-D model allows for analysis of a theoretical atmospheric column composition versus height over time and comparison of loss processes, such as reaction of N_2O_5 on aerosol particles versus the snowpack. Timescales for removal of NO_x are analyzed and model sensitivities to parameters and constraints are examined.

2 Model description

2.1 General features

The meteorological and microphysical part of MISTRA (MIcrophysical STRAtus) was originally a cloud-topped boundary layer model used for microphysical simulations of stratus clouds (Bott et al., 1996). MISTRA has been adapted as a marine and polar boundary layer model for studies of halogen chemistry (von Glasow et al., 2002; Piot and von Glasow, 2008) and includes gas phase, liquid phase, and heterogeneous chemistry, as well a microphysical module that explicitly calculates particle growth and treats interactions between radiation and particles. The full gas-phase reaction mechanism is available in the supplemental materials of Sommariva and von Glasow (2012), the aqueous mechanism is described in Pechtl et al. (2006), and photolysis rates are calculated online by the method of Landgraf and Crutzen (1998). Aerosol particles are initialized as the sum of

three log-normal modes based on the Jaenicke (1993) "urban" model and distributed into 70 bins by diameter. We note that these particles show a peak in the surface area distribution in the submicron range, where mass transport (diffusion) limitations to heterogenous reactivity are less important than the reactive uptake coefficient. Calculations of kinetic rates are governed by IUPAC (International Union of Pure and Applied Chemistry) rate constants. Mixing is driven by turbulent heat exchange coefficient calculations. The model has 150 vertical layers from the bottom layer centered at a height of 5 m to the model top at 2000 m. The bottom 100 layers are spaced with a 10 m vertical resolution while the top 50 layers are spaced logarithmically. The model runs have a 10 s integration time with output every 15 min. For a more detailed description of the model see von Glasow et al. (2002).

MISTRA treats dry deposition of gases to the snowpack as an irreversible removal from the lowest atmospheric layer (5 m) to the snowpack below using a resistance model presented by Wesely (Wesely, 1989; Seinfeld and Pandis, 2006). The parameterization includes aerodynamic, quasi-laminar, and surface resistance and utilizes gas – aqueous equilibrium coefficients explicitly calculated for each species by MISTRA. Parameters for a mixed forest with wetland in a winter, sub-freezing environment were chosen (Wesely, 1989) and include resistance to deposition by buoyant convection and a lower ground "canopy" to simulate resistance to uptake by leaves, twigs, and other exposed surfaces. No resistance to deposition by large vegetation resistance is included. A dry deposition velocity of 0.59 $\mathrm{cm\ s^{-1}}$ is explicitly specified for $\mathrm{N_2O_5}$, based on the field study by Huff et al. (2011), while all other dry deposition velocities are calculated using the parameterization by (Wesely, 1989). Significant dry deposition in the model occurs for species of interest $\mathrm{NO_2}$, $\mathrm{O_3}$, $\mathrm{N_2O_5}$, and $\mathrm{HNO_3}$. The dry deposition velocity for NO is calculated in MISTRA with the Wesely formulation but is unimportant, as found by Wesely and Hicks (2000).

The parameterization presented by Bertram and Thornton (2009) is used to calculate the accommodation coefficient, α, which is used in Eq. 4 of von Glasow et al. (2002) to calculate the heterogeneous uptake rates of $\mathrm{N_2O_5}$ for each aerosol particle size bin in each model layer as a function of time. The difference in the resulting heterogeneous rate coefficient between this approach and using γ in the simple equation $k = \gamma \bar{v} A/4$ is less than 10% but it allows us to use a model consistent way to calculate heterogeneous rate coefficients. Compared to the old approach as used in von Glasow et al. (2002), where $\alpha = 0.1$, the heterogeneous uptake rates of $\mathrm{N_2O_5}$ are now up to a factor of $20\times$ slower. The Bertram and Thornton (2009) parameterization is dependent on aqueous $\mathrm{NO_3^-}$ concentration, aqueous $\mathrm{Cl^-}$ concentration, and aerosol particle liquid water content. This parameterization was chosen because it includes the nitrate effect and formation of nitryl chloride through chemical concentrations available in the model's aerosol formulation. Although the organic component of aersol particles is significant, we have little observational details about the properties of this organic matter; for instance, we do not have the O:C ratio characterized, nor do we have any detailed information about mixing state. Therefore, it was not possible to model the effect of the organic component of aerosol particles on γ. The only wintertime field study of γ (Wagner et al.,

2013) indicated that the Bertram and Thornton (2009) model was reasonably close to observations, sometimes having the model underpredict observed γ values and unlike warmer climate studies that indicate organics poision heterogeneous reactivity (e.g. Bertram et al., 2009; Riedel et al., 2012; Ryder et al., 2014).

To simulate a high-latitude atmospheric column moving in space, MISTRA is initialized with a clean Arctic air mass that then receives a pollution injection for two hours, corresponding to the contact time of an air parcel moving over Fairbanks at a speed of about $1\,\mathrm{m\,s^{-1}}$. Model runs begin at local midnight ($t = 0$ h), with pollution injection period beginning at $t = 2$ h and ending at $t = 4$ h. Injection occurs as a positive flux from the ground surface into the lowest model layer ($5\,\mathrm{m}$). No additional injection occurs after $t = 4$ h and simulations continue until $t = 50$ h for analysis two days "downwind" of the pollution source to focus on the fate of emitted $\mathrm{NO_x}$.

2.2 Observational constraints

Model runs did not attempt to simulate a specific day for comparison with observations, but rather typical conditions are presented to study the detailed chemical processes occurring under idealized conditions. The "base case" scenario is initialized as an average November day with a clear sky and snow covered ground with an albedo of 0.8. Photolysis rate calculations are performed online for 10 November at latitude 64.76° N, with a sunrise of 8:03 AKST and a sunset of 15:57 AKST. Both daytime and nighttime chemistry occur in the model. Photolysis rate calculations use a total column ozone of 401 Dobson Units based the average of November 2009 observations over Fairbanks from the Total Ozone Mapping Spectrometer (TOMS, 2011). An initial temperature at ground level of $257\,\mathrm{K}$ (Fig. 2) is an observational average from 1929–2010 for November (ACRC, 2011). Relative humidity (RH) is initialized to 78 % in the mixed layer for the base case (Fig. 2) based on average of November 2009 observations from the meteorological station located at the Fairbanks International Airport courtesy of the National Climate Data Center (NCDC, 2011).

Vertical mixing at high latitudes can become extremely hindered due to temperature inversions caused by strong radiative cooling from the ground surface at night. We know of no nocturnal vertical profiles of $\mathrm{NO_x}$ species above Fairbanks in November, but a nocturnal in-situ vertical profile of $\mathrm{NO_2}$ was obtained in early April from the Arctic Research of the Composition of the Troposphere from Aircraft and Satellites (ARCTAS) campaign was available and also represents typical wintertime (inverted) conditions. Therefore, the ARCTAS $\mathrm{NO_2}$ profile is used to constrain chemical vertical profiles in such conditions (ARCTAS, 2008). The flight originated at Fairbanks International Airport and took off at 02:23 AKST on 8 April 2008. $\mathrm{NO_2}$ was detected to an altitude of $300\,\mathrm{m}$ along a flight path to the southwest, away from and downwind of downtown Fairbanks. The temperature profile obtained from the 8 April 2008 flight showed a surface inversion to $50\,\mathrm{m}$ and a capping inversion at $300\,\mathrm{m}$. Vertical mixing in stable conditions often presents problems in model simulations (e.g. Anderson and Neff, 2008) and our simulations suffer from this as well. Attempts to simulate

chemical profiles based on temperature profile observations did not yield results that agreed with the chemical profiles. Therefore, a mixed layer of 300 m is initialized using a dry-adiabatic lapse rate from the ground capped by a small isothermal layer (Fig. 2). The modeled vertical temperature profile allows for mixing of NO_2 to agree with the observed chemical vertical profile.

The chemical composition of the modeled atmospheric column at $t = 0$ h represents an unpolluted Arctic air mass. Ambient ozone mixing ratios from Barrow, Alaska are 35 $\mathrm{nmol\,mol^{-1}}$ on average from 2000–2010 in November, with peak abundances of 42 $\mathrm{nmol\,mol^{-1}}$ (ESRL, 2011) and concentrations of polar aerosols found close to the surface are generally very low (Seinfeld and Pandis, 2006). Therefore, the background chemical composition of the model is initialized as devoid of anthropogenic pollutants with an O_3 mixing ratio of 40 $\mathrm{nmol\,mol^{-1}}$ and an aerosol particle loading of $< 1\,\mathrm{\mu g\,m^{-3}}$.

The pollution injection during the "emission period" consists of NO, sulfur dioxide (SO_2), ammonia (NH_3), and aerosol particles containing organic matter, trace chloride (Cl^-), and SO_3 that rapidly hydrolyses to sulfuric acid (H_2SO_4) (Table 1). Sufficient NO emissions can "titrate" an air mass through Reactions (R1) and (R2), depleting O_3 and leading to an environment with excess NO, which is observed almost nightly in winter months in downtown Fairbanks (State of Alaska, 2008). The modeled NO flux is the smallest emission rate possible to titrate ozone to near zero through Reactions (R1) and (R2). This yields a modeled NO_x mixing ratio of 58 $\mathrm{nmol\,mol^{-1}}$ at the end of the pollution injection period ($t = 4$ h), which is within the first quartile (Q1) to third quartile (Q3) range of 31–103 $\mathrm{nmol\,mol^{-1}}$ from observations in downtown Fairbanks (State of Alaska, 2008) and simultaneously brings O_3 down to 1 $\mathrm{nmol\,mol^{-1}}$ at ground level. Emission of SO_2 is constrained by November 2008 average abundance observed in downtown Fairbanks (State of Alaska, 2008).

Ammonia and aerosol particle emissions are interrelated. Modeled aerosol particles are emitted as liquid particles containing organic material, highly oxidized sulfur species (e.g. SO_3 that rapidly hydrolyses to sulfuric acid, H_2SO_4), and trace amounts of chloride and are constrained by $PM_{2.5}$ (aerosol particles with aerodynamic diameter $< 2.5\,\mathrm{\mu m}$) observations of particulate organic matter, sulfate, and chloride from downtown Fairbanks (ADEC, 2007) (Table 1). To obtain an appropriate aerosol number density and surface area, the number density of a standard tri-modal urban aerosol distribution (Jaenicke, 1993) is scaled to agree with the average $PM_{2.5}$ mass observation for November (ADEC, 2007). Sulfate (SO_4^{2-}) concentrations from emitted highly oxidized sulfur species (e.g. SO_3 leading to H_2SO_4) are constrained on a percent mass basis based on total $PM_{2.5}$. The remaining observed aerosol particulate mass is primarily composed of organic carbon, elemental carbon, and heavy metals and is accounted for in the model using chemically inert dissolved organic matter.

Currently, there are no known ammonia observations in Fairbanks. Ammonia mixing ratios in remote areas can be $< 50\,\mathrm{pmol\,mol^{-1}}$ (Finlayson-Pitts and Pitts, 2000), so background NH_3 is initialized as 0.05 $\mathrm{nmol\,mol^{-1}}$. Biomass burning is a well documented source of ammonia emission (Yokelson et al., 1996, 1997; Akagi et al., 2011), suggesting combustion in woodstoves is a sig-

nificant NH_3 source. Emission of ammonia is constrained based on ratios of CO and NO_x emissions using Environmental Protection Agency (EPA) emission inventories and calculations based on previous studies. Carbon monoxide is produced from both automotive emissions and smoldering combustion in woodstoves. The automotive fraction comes at least partially from cold starts and poor operation at cold temperatures. These cold-weather-related emissions have been targeted and the automotive CO source has decreased, with the last exceedance of National Ambient Air Quality standards for CO in 1999, implying that woodstove emissions are now a larger fraction of CO emissions. Studies of smoldering combustion composition by Yokelson et al. (1997) have shown ammonia is the primary nitrogen emission from a smoldering fire and estimate NH_3 emissions from burning wood to be 10.8 % of the CO emission for white spruce harvested in Alaska. Recent Southern California emissions of ammonia related to automotive operations have been found to be somewhat smaller at $3.3 \pm 1.3\%$ mol NH_3 / mol CO (Nowak et al., 2012). However, emissions of CO in Fairbanks are related to cold-weather not experienced in California, so the emissions ratio may be different. Therefore, we used the larger smoldering combustion emissions ratio as an estimate of combustion-related ammonia emissions. The EPA emissions inventory for Fairbanks in 2005 listed 1325 $\mathrm{tons year}^{-1}$ (TPY) of carbon monoxide (CO) (ADEC, 2008). Assuming all smoldering combusion emissions are produced in the winter 6 months out of the year, this yields an estimate of 221 $\mathrm{tons month}^{-1}$ (TPM) of CO. Assuming local fuel is consumed in woodstoves, the estimation using Yokelson et al. (1997) would yield 24 TPM NH_3, currently not accounted for in the emissions inventory. For mobile sources, the emissions inventory reports 71 TPM NO_x and 4 TPM NH_3 from annually occurring on-road, gasoline-powered sources. Calculations based on results from a study by Kean et al. (2000) suggest the magnitude of NH_3 emissions are 25 % that of NO_x from automobiles due to use of 3-way catalyst systems in gas-powered vehicles. By this estimate, on-road NH_3 from gas-powered vehicles is 18 TPM, an estimate 4.5 times higher than the NH_3 value listed in the inventory. Together, these estimates of NH_3 emissions from woodstoves and automotive sources make for 42 TPM NH_3, which is 4.8 % of the total reported NO_x emission of 872 TPM. Therefore, the ammonia flux during the emission period in the base case is constrained to be 4.8 % by mass of NO_x emissions. Using the Nowak et al. (2012) California automotive ammonia / carbon monoxide emissions ratio and associating all wintertime CO with automotive emissions and no woodstove ammonia would lead to about 7 TPM automotive NH_3, again significantly higher than in the inventory, but lower total emissions than in the base case. We will address this uncertainty in ammonia emissions through sensitivity studies.

Another constraint on ammonia emissions comes from observed aerosol particle ammonium. Ammonia (NH_3) readily protonates in acidic particles to form ammonium (NH_4^+), increasing the pH. The molar ratio of NH_4^+/SO_4^{2-} in aerosol particles can be used to determine aerosol acidity, where a value above 2 indicates that all sulfuric acid has been neutralized. Data from downtown Fairbanks shows the first to third quartile range of molar NH_4^+/SO_4^{2-} to be 1.5–2.4 (State of Alaska, 2011).

Modeled NH_3 emission from the ground, as explained above, is ~ 3 times the molar H_2SO_4 emission, thus enough NH_3 is emitted to neutralize the sulfuric acid. Smaller emissions of ammonia become insufficient to neutralize sulfate aerosol particles, although sensitivity studies are carried out down to levels of ammonia emission five times below the base case.

3 Results

3.1 The urban pollution plume

The evolution of modeled primary emissions, destruction of ozone, and resulting products are shown in Figs. 3 and 4. All pollutants rapidly mix upon emission to 100 m at $t = 4$ h, reaching 300 m at approximately $t = 8$ h, then slowly dilute higher for the duration of the model run. The NO_x vertical profile (Fig. 3a) shows a strong decrease with height at the end of the emission period due to ground level emission. Emitted NO_x reaches 100 m altitude at the end of the emission period ($t = 4$ h) and 300 m, the top of the initialized mixed layer, within 2 h after emissions cease ($t = 6$ h).

Modeled total $PM_{2.5}$ (Fig. 3b) shows a vertical profile similar to NO_x in the first two hours after the emission period ends ($t = 6$ h) due to vertical dilution. No observations of aerosol number density and surface area are available for downtown Fairbanks for model evaluation. Modeled values at ground level at $t = 4$ h reach a number density of $2 \times 10^4\ cm^{-3}$ and aerosol surface area density of $380\ \mu m^2 cm^{-3}$. Modeled nitrate produced through secondary formation by Reaction (R4a) and (R4b) in aerosol particles is 2 % of total $PM_{2.5}$ mass at $t = 4$ h, compared to an average observed value of 4.4 % total $PM_{2.5}$ mass in November (ADEC, 2007). Background and emitted ammonia rapidly react with emitted acidic aerosol particles, forming particulate ammonium (Fig. 4f). Modeled ammonium in aerosol particles is 5 % by mass at $t = 4$ h, and closely resembles ammonium observations comprising 6.4 % of total $PM_{2.5}$ mass (State of Alaska, 2011). Particulate ammonium formation leads to values of NH_4^+/SO_4^{2-}=1.5 (Table 1) at the end of the emission period ($t = 4$ h) through aerosol particle uptake and increases the molar ratio of NH_4^+/SO_4^{2-} to 2.1 one hour after the emission period ($t = 5$ h). Column integrated SO_2 remains constant in time, indicating that the model does not produce significant amounts of sulfate from oxidation of SO_2 in the base case, and the only loss mechanism of SO_2 from the atmosphere is dry deposition (not shown).

3.2 Plume evolution in the base case

Previous field studies in Fairbanks were performed outside of the downtown area in order to observe un-titrated air masses that allow for formation of N_2O_5. Ayers and Simpson (2006) conducted measurements on the edge of the populated area of Fairbanks and observed both titrated and un-titrated air masses. Modeled dilution of NO_x (Fig. 3a) agrees well with various field measurements in the greater Fairbanks area (Table 2), where abundances of NO_x reduce with distance from downtown.

Background ozone (Fig. 4a) is depleted ($< 2\,\mathrm{nmol mol^{-1}}$) at ground level at $t = 4$ h and is significantly reduced in the mixed layer due to titration of the air mass through Reactions (R1) and (R2). Ozone abundance returns to near background approximately four hours after the pollution injection due to vertical mixing and photolysis of NO_2 in daylight hours.

Abundance of N_2O_5 in the model (Fig. 4b) peaks aloft in the early morning of the first day ($t = 9$ h) and in the middle of the second night (beginning $t = 21$ h). The diurnal cycle of N_2O_5 shows it is not produced during daylight hours but peak levels can be maintained for about one day after NO emissions cease from the remaining NO_x in the atmosphere. A reduction in mixing ratio of N_2O_5 near the ground occurs due to dry deposition to the snowpack. Modeled abundance of N_2O_5 agrees well with observations by Ayers and Simpson (2006), but modeled N_2O_5 near the ground is overestimated at longer distances (Table 2). This result is consistent with enhanced N_2O_5 deposition to vegetation and enhanced turbulence due to surface vegetation and is discussed in Sect. 5.1.

Formation of $ClNO_2$ (Fig. 4c) occurs immediately upon formation of N_2O_5 through Reaction (R4b) and removes trace Cl^- in emitted aerosol particles (not shown) in less than one hour after emissions end ($t = 5$ h). A reduction in N_2O_5 mixing ratio below 50 m can be seen (Fig. 4b) from $t = 4$ h to $t = 5$ h that is due to $ClNO_2$ formation. Once formed, $ClNO_2$ dilutes through the mixed layer and abundances of $\sim 20\,\mathrm{pmol mol^{-1}}$ throughout the mixed layer are lost through photolysis during the first day resulting in peak Cl radical concentrations of $2.6 \times 10^3\,\mathrm{radicals cm^{-3}}$. Formation of $ClNO_2$ is limited by aqueous Cl^- concentrations in this simulation.

Particulate nitrate (Fig. 4d) is primarily formed through Reaction (R4a) and peaks ~ 24 h after the emission period at the end of the second night, corresponding to reactive uptake of N_2O_5 formed during the second night. Total nitrate (all aerosol particle sizes) peaks at a concentration of $6.0\,\mu\mathrm{g m^{-3}}$ at an altitude of 325 m at $t = 30$ h, where $4.2\,\mu\mathrm{g m^{-3}}$ of the nitrate is in the $PM_{2.5}$ size fraction. Concentrations of nitrate at ground level reach a maximum of $2.2\,\mu\mathrm{g m^{-3}}$ about 16 h after emission ends, showing a delay in secondary formation of nitrate through the dark oxidation pathway. Gas phase nitric acid (Fig. 4e) mixing ratio peaks within hours after the nitrate aerosol peaks and is outgassed by particles made acidic through Reaction (R4a). Larger aerosol particles are able to uptake greater amounts of NO_3^-. The peak number density of large aerosol particles ($d > 2.5\,\mu\mathrm{m}$) occurs aloft, leading to increased NO_3^- aloft (Fig. 4d) and decreased abundance of gas-phase HNO_3 aloft (Fig. 4e). The modeled HNO_3 does not react readily with other species and will be ultimately removed through aerosol uptake upon mixing or deposition to the snowpack.

Formation of NH_4^+ (Fig. 4f) occurs during the emission period and one hour immediately following emission due to aerosol particle uptake of NH_3 and neutralization of emitted sulfuric acid aerosol particles. This process depletes background ammonia and emitted ammonia throughout the column (not shown) and forms ammonium sulfate [$(NH_4)_2SO_4$] or ammonium nitrate (NH_4NO_3) in the particles. Once ammonium in formed in the aerosol particles they are well-mixed throughout the mixed layer and no losses from the atmosphere exist except aerosol particle deposition to the

snowpack. Some additional ammonium is produced after the emission period due to entrainment from background ammonia above the mixed layer.

3.3 Fate of NO_x in the base case

Nitrogen speciation is divided into four categories (Fig. 1) to characterize the state of emitted NO_x in time. Gas-phase nitrogen oxide species that have not yet undergone heterogenous reaction on aerosol particles (R4a and R4b) are grouped into the term "un-reacted", which is not meant to imply no reaction but simply no irreversible heterogenous conversion to nitrate-type species. The "un-reacted" fraction includes NO_x, NO_3 (which is very small due to reactivity) N_2O_5, and other reactive nitrogen species present in sub-$\mathrm{pmol\,mol^{-1}}$ range: HONO, and HNO_4. The "aerosol reacted" fraction includes any aqueous phase NO_3^-, HNO_3 formed by nighttime chemistry then outgassed from acidic particles, and $ClNO_2$ that remains suspended in the atmosphere. The "N_2O_5 dry deposited" fraction represents dry deposition of N_2O_5 only. The "other deposited" fraction includes dry deposition of NO_2 and HNO_3 and deposition of NO_3^- aerosol. Reduced species NH_3 and NH_4^+ are not oxidized under simulation conditions and are not included in the speciation analysis.

Figure 5 presents a time series of speciation of emitted NO_x, depicted as the column integrated fraction of each species out of the total emitted NO_x. Diurnal cycles discernible include the formation of NO and destruction of N_2O_5 during the day. A vertical transect at any point in time depicts the current state of emitted NO_x. Most apparent is the trend of the un-reacted fraction decreasing with time. In the base case, only 36 % of un-reacted nitrogen remains in the atmosphere two days after the beginning of emissions ($t = 50$ h), with the remaining 63 % partitioned among the other categories (Fig. 5). The large fraction of gas phase HNO_3 (33 % at $t = 50$ h) is due to acidic aerosol conditions and represents a significant fate of emitted NO_x. Night-time formation of HNO_3 dominates gas phase HNO_3 production, but a small amount of HNO_3 production can be seen in the afternoon periods due to the daytime oxidation pathway. Dry deposition of HNO_3 through the aerosol reacted pathway is the fate of 5 % of the total emitted NO after two days, but is less than the N_2O_5 dry deposited fraction of 17 %. Dry deposition of N_2O_5 makes up a discernable fraction two hours after the emission period ends while NO_3^- aerosol deposition and HNO_3 dry deposition does not build until 16 h after the emission period ends. A slight increase in dry deposition occurs during the day due to increased turbulent mixing. Other reactive nitrogen species such as HONO, HNO_4, and N_2O_4 are included with the NO_2 fraction and make up an insignificant portion (< 1 %).

4 Sensitivity of the fate of NO_x to model parameters

Experiments were performed to analyze the sensitivity of the fate of NO_x to model constraints by modifying parameters over ranges based on realistic conditions. These experiments are presented as demonstrations of model performance as well as representations of the base case under changing

scenarios. Sensitivities found to be most significant are described below and are depicted in Fig. 6a–h. Analysis of each experiment is conducted by relative comparison of total nitrogen fractions in each speciation category two days after the emission period ends ($t = 50$ h).

4.1 NO emission rate

Increased flux of NO during the emission period leads to increased NO_x abundance, most intensely near the ground. Increased mixing ratio of NO depletes O_3 in the mixed layer, slowing Reactions (R1) and (R2) and N_2O_5 formation. This slowing of N_2O_5 formation causes the un-reacted fraction to remain dominant. The $5\times$-NO case represents a strongly titrated air mass. In this case, modeled NO_x reaches $300\,\mathrm{nmol\,mol^{-1}}$ at $t = 4$ h, within the range of downtown observations (Table 1), leaving excess NO and depleted ozone at night throughout the mixed layer for the entire duration of the run, suppressing N_2O_5 formation and slowing nocturnal oxidation of NO_x. Alternatively, under a lower NO emission rate, NO_x is efficiently removed through the dark oxidation pathway, with preference for the aerosol reacted fraction.

4.2 NH_3 emission rate

Increased emissions of NH_3 lead to greater amounts of NO_3^- retention in the particulate phase, giving increased particulate surface area and thus a greater aerosol reacted fraction. This result was somewhat surprising because we expected that the increased nitrate effect from enhanced NO_3^- retention would decrease the reactive uptake coefficient, according to the parameterisation by Bertram and Thornton (2009), and reduce the aerosol particle reactivity. However, the heterogeneous uptake rate is not only determined by nreactive uptake limitations and in this case larger available reactive surface area outweighs the reduction in the reactive uptake coefficient due to the nitrate effect. This sensitivity is discussed further in Sect. 5.3.

4.3 Aerosol emission rate

In general, increased aerosol flux from the surface leads to greater aerosol particle number density, surface area, and mass density of sulfate particles. Primary sulfate emissions do not leave the particles and thus lead to increased total aerosol particle mass. The increase in aerosol particle surface area allows for more surface reactivity and increases the aerosol reacted fraction and aerosol particle deposition in the other deposited fraction over the $1/5\times$–$5\times$ factor sensitivity experiments. Additionally, the N_2O_5 dry deposited fraction is decreased due to the enhanced aerosol uptake. The decrease of the aerosol reacted fraction in the $2\times$ experiment requires further examination, but is likely a feedback based on NO_x emission and time of analysis ($t = 50$ h).

As discussed in the introduction, the reactive uptake coefficient calculation model (Bertram and Thornton, 2009) may overestimate reactive uptake rates, particularly in the case where organic components coats particulate surfaces. Because the rate of N_2O_5 heterogeneous hydrolysis is dependent

upon both the aersosol particle surface area and the reactive uptake coefficient, the effect of increasing the latter is likely to be similar to increased aerosol particulate emission. Therefore, we would expect that if the actual reactive uptake coefficient is lower than calculated by Bertram and Thornton (2009), as has been observed in the presence of organic coatings (Bertram et al., 2009; Riedel et al., 2012; Ryder et al., 2014), the aerosol reacted fraction would decrease. Alternatively, if the actual γ is larger than modeled, as has been observed at times during the wintertime study of Wagner et al. (2013), the aerosol reacted fraction would be expected to increase.

4.4 $\mathbf{N_2O_5}$ dry deposition velocity

The empirical value of dry deposition velocity of N_2O_5 was found to be between 0.12–1.06 cms^{-1} (Huff et al., 2011) and covered by the range of the $1/5\times$–$2\times$ sensitivity experiments. The total fraction of N_2O_5 dry deposited varies from 5 % to 25 % over this range. Increases in the dry deposition velocity of N_2O_5 lead to an increase in the N_2O_5 dry deposited fraction, a corresponding decrease in all other fractions, and a reduction of N_2O_5 mixing ratio at ground level, near the snowpack.

4.5 Photolysis

In this experiment, photolysis calculations are carried out for 10 November, 21 December, 22 January, 21 February, and 20 March. The lowest photolysis rate (21 December) corresponds to the smallest un-reacted fraction. Under the weakest photolysis conditions, N_2O_5 is present at all hours and reaches a minimum value of 200 $\mathrm{pmolmol}^{-1}$ throughout the mixed layer during the day. This N_2O_5 abundance allows for nitrate formation via the dark oxidation pathway through Reaction (R3) for 24 h per day. Increased photolysis and longer periods of daylight (20 March) leads to an increased un-reacted fraction due to limitation of Reaction (R3) during the shorter nights and weak daytime oxidation of NO_x. Monthly average temperatures in winter in Fairbanks are very similar due to large temperature fluctuations over a monthly time period, and each month is likely to have days near the base case temperature of 258 K. For a sensitivity experiment with respect to temperature, see (Sect. 4.7).

4.6 Initial RH

This experiment modifies the initial RH in the mixed layer. Increases in RH lead to increases in aerosol surface area from water vapor to particle equilibrium, which is calculated by the model. Most substantial in a relatively dry mixed layer, a 20 % increase in RH from 40 % to 60 % increase the aerosol reacted fraction by 9 %.

4.7 Surface temperature

For this experiment, temperature at bottom layer of the atmosphere ranges from 228 K to 273 K, which could occur on any given day during the months of November to March. Decreasing temper-

atures produce a significantly greater un-reacted fraction due to kinetic limitation of reactions.

4.8 Initial mixing height

The mixed layer in the model gradually rises in time (Fig. 2) due to mixing from above. Due to the time needed to mix air throughout the 300 m mixed layer (~ 6 h), the height of the mixed layer is nearly constant at 100 m at the end of the emission period for all runs (100–400 m) and therefore does not affect constrained mixing ratios of emissions. Thus, this experiment shows variation of the dilution downwind of the emission source due to a variable mixed layer height. Increases in the height of the mixed layer decrease both N_2O_5 dry deposited and other deposited fractions while increasing the amount of aerosol reacted fraction retained in the atmosphere due to less contact with the snowpack surface.

4.9 Chloride concentration (not shown)

In this experiment, aqueous concentration of emitted chloride in aerosol particles varies from zero–$5\times$ base to determine the effect on NO_x. This range leads a particulate chloride concentrations of 0.00–0.56 $\mu g m^{-3}$ at $t = 4$ h near the ground. These trace amounts of Cl^- present in the particles slightly reduce the aerosol reacted fraction, while the aerosol-reacted fraction increases by 3 % when no Cl^- is included. This weak sensitivity of the fate of NO_x to particulate chloride is likely due to analysis occurring two days after emission. Analysis less than eight hours after emissions end yielded a larger sensitivity to Cl^- due to the presence of $ClNO_2$ in the aerosol reacted fraction. Significant reductions in N_2O_5 mixing ratio and nitrate production are seen (Fig. 4b) in the first hours after emission ends due to production of $ClNO_2$. Therefore, aerosol chloride concentrations may have a much greater impact on a local scale.

4.10 Time of day (not shown)

The start of the emission period was varied to analyze the effect of photolysis on the fresh or aged plume. With respect to local impacts (under 8 h), time of day has a significant effect on column composition by hindering or allowing the dark oxidation pathway to occur immediately after emission. Therefore, time of day of NO_x emission is found to have a significant effect on N_2O_5 deposition on a local scale, where NO_x emissions in daylight are likely to travel farther from the source before undergoing oxidation and NO_x emissions at night will enhance local deposition. By $t = 50$ h, however, the plumes are exposed to approximately equal amounts of sunlight and there is no significant effect on the fate of NO_x.

4.11 SO_2 emission (not shown)

Weak photolysis conditions in the base case do not allow for significant secondary formation of sulfate by SO_2 oxidation by the OH radical. Therefore, SO_2 is virtually inert in these simulations

and does not affect the fate of NO_x.

4.12 Deposition to canopy (not shown)

An additional experiment was performed to include the "upper canopy" term (see Seinfeld and Pandis, 2006) of mixed forest in the dry deposition parameterization to simulate deposition to trees. Addition of an upper canopy parameter in the dry deposition equation leads to increases of dry deposition velocity of 10 % for HNO_3, 16 % for NO_3, and an order of magnitude for NO_2. The explicitly set value for dry deposition velocity of N_2O_5 is scaled up by 10 % for this experiment, based on the result for HNO_3. Including the upper canopy results in a 4 % increase in the other deposited fraction, primarily due to increased NO_2 deposition, and a < 1 % increase in the N_2O_5 dry deposited fraction. In this 1-D model, addition of deposition to the upper canopy of trees has an insignificant effect on the fate of NO_x. However, air transport over horizontally varying trees causes mixing of surface and near-surface layers that may enhance deposition in a way we cannot model in this 1-D simulation. This point is discussed below.

5 Discussion

5.1 Local effects vs. long-range transport

Results from the base case speciation analysis (Fig. 5) have implications for local and long-range deposition effects. Dry deposition of N_2O_5 begins immediately upon formation of N_2O_5 and dominates the nitrogen flux to the snowpack during the night. Snowpack deposition of aerosol nitrate and gas-phase HNO_3 does not occur in significant amounts until 16 h after emissions have ended. This indicates dry deposition of N_2O_5 dominates nitrogen deposition to the snowpack on a local scale, while particulate nitrate deposition is minimal. Alternatively, particulate nitrate can remain suspended in the local atmosphere, undergo long-range transport, be diluted in transit, and removed by a precipitation event.

Observations of both titrated and un-titrated air masses in studies such as Ayers and Simpson (2006) indicate a wide variability of the oxidation capacity of the mixed layer. Sensitivity experiments presented here have shown NO emissions in the absence of photolysis can transform the lower atmosphere from an oxidizing environment rich in ozone to a reduced environment with no oxidation capacity. Some values of NO_x observed in downtown Fairbanks are even greater than the modeled $5\times$-NO_x experiment (Fig. 6a) in which ozone was titrated in the mixed layer for two days. In reality, horizontal mixing may reduce the timescale of titration as background ozone is mixed in, but ozone reduction may linger for well over 24 h downwind. Ozone titration is likely to be enhanced under stable meteorological conditions.

The photolysis experiment (Fig. 6e) has implications for environments at higher latitudes than Fairbanks, which is located at 64.76° N. The month of December, with the weakest photolysis and

longest periods of darkness, shows the smallest un-reacted fraction. Dry deposition of N_2O_5 and aerosol reacted fractions are enhanced by extended darkness. Locations north of the Arctic Circle (66.56° N) will have days on which no photolysis will occur and N_2O_5 formation is occurring continuously, allowing the dark oxidation pathway of NO_x to be active 24 h per day. Under total darkness conditions, local deposition of N_2O_5 is likely to be enhanced.

The drastic dependence of the fate of NO_x on temperature (Fig. 6g) shows ambient temperatures are the most important naturally-occurring factor controlling the chemistry of the nocturnal NO_x plume. The primary reason for the increased "unreacted" fraction is that the formation rate of NO_3 slows at colder temperatures, leaving a larger fraction of NO_x unreacted at the $t = 50$ h analysis time. Interestingly, dry deposition rates of N_2O_5 remain fairly constant over this temperature range. The range of temperatures studied are not uncommon in Fairbanks for the months of November to March. For temperatures lower than 228 K and stable meteorological conditions, NO_x may be near the snowpack for extended periods of time, possibly enhancing dry deposition.

5.2 Vertically varying chemistry

Modeled vertical profiles of N_2O_5 have implications for interpreting field measurements. Modeled N_2O_5 mixing ratio at 105 m one hour immediately following the emission period ($t = 5$ h) is over $2\times$ greater than at the surface and consistently 10–15 % greater for the duration of the model run. This suggests that observations carried out near the snowpack may yield abundances of N_2O_5 significantly lower than those aloft. More importantly, positive vertical gradients of N_2O_5 reaffirm the result found by Huff et al. (2011) that dry deposition is a significant loss mechanism of N_2O_5 near the snowpack.

Additionally, loss of N_2O_5 near the ground may be underestimated. Modeled values of N_2O_5 aloft in the first hour after emissions end ($t = 5$ h) are in good agreement with measurements performed 80 m above the valley floor (Table 2). This suggests the model properly captures loss of N_2O_5 aloft on short timescales (a few hours). At longer distances and near the ground, the model predicts $\sim 4\times$ observed abundances of N_2O_5 (Table 2). The measured dry deposition velocity of N_2O_5 used to constrain the model was based on aerodynamic methods and measured above a treeless, flat snowpack. Under this constraint, the model assumes a flat ground surface for the entire model run, whereas Fairbanks is surrounded by densely wooded terrain, which enhances turbulence due to roughness. This turbulence is expected to enhance deposition of N_2O_5 and thus reduce observed N_2O_5 when compared to modeled values, which is a treeless environment free of mechanical turbulence.

The effect of enhanced turbulence near the ground would increase air parcel transport to the ground surface, with a result similar to that of a sensitivity experiment with enhanced dry deposition velocity of N_2O_5. The model scenario with an enhanced value of 2.95 cms^{-1} (Fig. 6d) still predicts N_2O_5 abundance near the ground $\sim 2\times$ greater than observed values. This method is not

the correct way to address enhanced deposition because deposition velocity is increased rather than air parcel contact with the snowpack. It does, however, suggest that deposition of N_2O_5 may be significantly underestimated in the treeless model scenario. Modeling enhanced deposition due to mechanical turbulence induced by a three-dimensional object such as tree cover is a limitation of the one-dimensional model. Airborne observations of N_2O_5 aloft, away from Fairbanks, would verify if the model properly captures loss of N_2O_5 away from the ground and would verify that loss to ground surface is underestimated. Such observations are necessary to fully understand the vertical and spatial distribution of the nocturnal nitrogen plume.

5.3 Ammonium nitrate formation

Downtown Fairbanks lies in a US Environmental Protection Agency non-attainment area for $PM_{2.5}$ (ADEC, 2008). A common concern in reducing total $PM_{2.5}$ lies in a non-linearity present in aerosols containing ammonium, nitrate, and sulfate. When excess ammonia is available (molar ratio of $NH_4^+/SO_4^{2-} > 2$), reductions in particulate sulfate may be replaced by particulate nitrate, leading to an increase of ammonium nitrate in the aerosol particles (Seinfeld and Pandis, 2006, p. 483). Modeled particulate nitrate concentrations in the polluted area ($t = 4$ h) are $< 0.5\,\mu g m^{-3}$ and agree with observations (ADEC, 2007), but concentrations of $> 2\,\mu g m^{-3}$ NO_3^- are modeled within six hours after emissions end. These results suggest that secondary particulate nitrate formation due to NO_x oxidation within Fairbanks urban core is not a major contributor to $PM_{2.5}$ non-attainment because titration of O_3 slows N_2O_5 formation and thus formation of NO_3^- and HNO_3. Enhanced secondary formation of particulate nitrate, however, may have implications further downwind of the polluted area.

In the NH_3 emission rate sensitivity experiment (Fig. 6b), the aerosol reacted fraction increases with increased ammonia emission. This effect can be seen in total $PM_{2.5}$ concentrations near the ground (Fig. 7) beginning two hours after end of emission due to formation of ammonium nitrate (NH_4NO_3). During the emission period, primary emissions of fully oxidized sulfur leading to H_2SO_4 and organic matter dominate total mass and are similar for each experiment. During the emission period and for ~ 2 h afterward, NH_4NO_3 concentrations are zero and $NH_4^+/SO_4^{2-} < 2$ in the particle and sulfuric acid is not fully neutralized. Base case emissions of NH_3 are sufficient to bring the molar ratio of NH_4^+/SO_4^{2-} at the surface to 1.5 at $t = 4$ h, which gradually increases to 2.1 at $t = 5$ h. Values of $NH_4^+/SO_4^{2-} > 2$ are possible as NO_3^- is formed and available to react with NH_4^+ to form NH_4NO_3 (Seinfeld and Pandis, 2006, p. 479). Increases in the NH_3 flux bring the NH_4^+/SO_4^{2-} ratio at the end of the emission period ($t = 4$ h) to 1.9 for the $5\times$ NH_3 run. Divergence of total $PM_{2.5}$ mass at $t = 8$ h (Fig. 7) between the sensitivity studies is controlled by NH_3 emission and subsequent formation of NH_4NO_3. In this manner, secondary formation of nitrate particles is controlled in magnitude by ammonia flux and the rate of nocturnal NO_x oxidation, which is strongly affected by ozone titration. In all cases, secondary aerosol mass continues to form during the first

day while N_2O_5 is still present from nighttime formation (Fig. 7). Dry deposition of ammonia gas competes with uptake of ammonia by aerosol particles and neutralization of particulate acidity, so in cases where vertical mixing is hindered, deposition of ammonia may also limit the uptake to aerosol particles.

The slow timescale of NH_4^+ uptake by aerosol forming NH_4NO_3 makes it impossible to infer NH_3 abundances downtown based on NH_4^+ measurements. Due to the slow timescale of nitric acid or particle nitrate formation, a decrease in primary sulfate emissions should reduce total $PM_{2.5}$ and not be replaced by an increase in particulate nitrate in the downtown area. However, this NO_x is later oxidized to HNO_3 and particulate NO_3^-, which later reacts with NH_3 forming NH_4NO_3 that could result in soil fertilization downwind of Fairbanks.

Constrained by emissions inventories and calculations, NH_3 emissions yielded a value of $0.96\,\mu g\,m^{-3}$ NH_4^+ and $1.6\,nmol\,mol^{-1}$ excess NH_3 near the ground at the end of the emission period ($t = 4$ h). In order to achieve the measured November average of $0.97\,\mu g\,m^{-3}$ NH_4^+ (State of Alaska, 2011) through aerosol uptake, we estimate a minimum of $1.2\,nmol\,mol^{-1}$ NH_3 need be available for uptake into aerosol particles. The base case emitted NH_3 was sufficient to reach NH_4^+ observations and yield excess NH_3. We believe automotive and woodsmoke sources of NH_3 are sufficient to account for measured NH_4^+/SO_4^{2-} ratio. Results of sensitivity experiments have shown NH_3 could be greater than modeled in the base case with no indication present in NH_4^+ observations downtown due to slow NH_4NO_3 formation caused by titration. However, if there are larger than base case ammonia emissions, significantly enhanced formation of NH_4NO_3 is modeled outside of the primarily polluted area. Therefore, observations of NH_3 emissions would be highly valuable for understanding Fairbanks air quality and possible downwind ecosystem impacts through ammonium nitrate deposition.

The origin and chemistry of sulfate aerosol in Fairbanks winter is currently unknown. The emissions used in this simulation, constrained by gas phase SO_2 and $PM_{2.5}$ SO_4^{2-} observations, estimate column integrated total sulfur is in the form of 93 % SO_2 and 7 % fully oxidized sulfur (e.g. SO_3) that rapidly reacts to form SO_4^{2-}. A value of 7 % is likely too high to be purely primary sulfate emission, but the modeled base case scenario produces no secondary sulfate from SO_2, which would be expected in an atmosphere with weak OH photochemistry and reduced oxidants (due to titration of ozone). Sulfur oxidation catalysis by transition metals has been presented as a sulfate formation mechanism (Brandt and van Eldik, 1995; Hoffman and Boyce, 1983) and could be a significant secondary SO_4^{2-} source during winter. If the formation of SO_4^{2-} by metal catalysis is fast, the sulfate could appear like true primary emissions, as we have modeled them in this study. The fate of NO_x emissions is found to be insensitive to SO_2, but this may not have been the case if secondary sulfate was formed by pathways alternative to photochemistry. Additional study would be useful for understanding the sulfate chemistry in Fairbanks and identifying possible remedies for $PM_{2.5}$ non-attainment.

5.4 Model limitations

The simulations in this experiment presented for analysis of the fate of anthropogenic NO_x pollution in a high-latitude environment are not without a few limitations. The meteorological conditions in the model were chosen such that cloud formation is avoided, primarily because microphysical and chemical feedbacks would hinder the main focus of this study, which was the fate of emitted NO_x in a high-latitude winter environment. Clear skies dominate synoptic conditions in the greater Fairbanks area in the winter months, supporting that the base case simulation is not weakened by the absence of clouds. Observations by Sommariva et al. (2009) found that that N_2O_5 removal by fog droplets was dominant when fog was present. Cloud formation would likely lead to dominance of N_2O_5 uptake aloft in large cloud particles, leading to less gas-phase HNO_3 and more nitrate aloft which could undergo long-range transport. Cloud formation would also affect photolysis rates in model layers below the cloud.

The temperature profile used to initialise the model was not taken from an individual measured profile but rather an idealised case because this idealized case better replicated the ARCTAS NO_2 profile. This model deficiency is a common problem for numerical models of the stable boundary layer (see discussion in Anderson and Neff, 2008). The NO_2 detected by the ARCTAS aircraft at $300\,\mathrm{m}$ was $14\,\mathrm{km}$ from downtown Fairbanks (ARCTAS, 2008). Assuming column motion of about $1\,\mathrm{ms}^{-1}$, $14\,\mathrm{km}$ would correspond to the modeled NO_x profile at $t = 8\,\mathrm{h}$, which shows vertical dilution to $\sim 290\,\mathrm{m}$. The modeled temperature profile of the base case is applicable for conditions with relatively high mixed layers and weak inversions, which are common in the "shoulder" months of October, November, March and April. Mixing due to the modeled temperature gradient is suitable for this study; however, mixing forced by eddy-diffusivity has been performed to match observed vertical profiles (Geyer and Stutz, 2004) and may be more appropriate for thermally inverted and stratified boundary layer simulations. However, vertically resolved chemical observations are required to apply the Geyer and Stutz (2004) method.

As MISTRA is a 1-D model, horizontal mixing is not included. This lack of horizontal mixing ensures that column-integrated abundances conserve mass, allowing the analysis shown here, while still explicitly allowing vertical mixing that is necessary to consider the competition between surface and aloft chemical processes. Horizontal mixing over the duration of the model runs will depend strongly on the prevailing synoptic situation so that a quantification of the effect of horizontal mixing is not possible. Horizontal mixing with background ozone would lead to less limitation of Reactions (R1) and (R2) and more efficient removal of NO_x.

Aerosol particles in the simulations were represented as purely aqueous constituents. With respect to frozen water, observations by LIDAR in Fairbanks indicate presence of super-cooled droplets in high-latitude environments at temperatures as low as $240\,\mathrm{K}$, suggesting aqueous phase aerosols are present in temperatures well below the freezing temperature of water (Fochesatto et al., 2005). Freezing of particles would have complex and currently poorly understood effects on reactivity.

However, freezing could potentially occur on the two-day timescale, implying that more study of the structure and reactivity of ice particles is needed.

Field observations have shown that the reactive uptake coefficient parameterization of (Bertram and Thornton, 2009) often results in γ values larger than observed in the field, which has been associated with organic aerosol content (Bertram et al., 2009; Riedel et al., 2012; Ryder et al., 2014). We had no observational constraints on the properties of the organic matter in the aerosol particles (e.g. internal/external mixing state, O:C ratio, etc.), so we could not enhance the γ calculation model. However, γ observed under wintertime conditions in the study of Wagner et al. (2013) was comparable to and sometimes exceeded the calculation method used here, possibly indicating that the Bertram and Thornton (2009) model is reasonably accurate under the conditions simulated here. The significant uncertainties that exist in proper calculation of γ need further study, and the study we report here indicates that airborne observations of N_2O_5 should be particularly sensitive to γ and aerosol particle properties.

6 Conclusions

Simulations have shown that approximately two-thirds of NO_x is lost in two days after emission in high-latitude winter conditions mostly through the dark oxidation pathway. Observed pollution fluxes commonly produce a reduced environment with excess NO and near zero ozone, slowing secondary oxidation chemistry that removes NO_x. The fraction of emitted NO_x that remains in the atmosphere was found to be most sensitive to the NO emission flux and temperature. Winter months with relatively warm temperatures and high mixing heights are likely to have the greatest nitrate aerosol particulate loading. Alternatively, cold days with low mixed layers are likely to have the greatest dry deposition rates and greatest local nitrogen deposition impact. Dry deposition rates of N_2O_5 were found to be most sensitive to aerosol surface area and dry deposition velocity, illustrating the competition between dry deposition and aerosol reactivity for removal of N_2O_5. Due to ground contact only occurring in the bottom model layer, greater amounts of total emitted NO_x were removed from the column via aerosol particle reactions (38 %) than through dry deposition (17 %) two days after emission in the base case scenario. Modeled abundances of N_2O_5 showed diurnal variations of over 1000 % and positive vertical gradients from the snowpack, showing the need for further study to understand vertical distribution of the emission plume and estimate potential impacts.

Acknowledgements. The authors would like to thank NOAA for use of the Ferret program for analysis of model output and UCAR for the use of NCL plotting software, which was used to generate the figures in this manuscript. The authors would like to thank Deanna Huff and Barbara Trost with the Alaska Department of Environmental Conservation and Jim Connor with the Fairbanks North Star Borough Air Quality Division for collaboration and providing observational data. Thanks to Catherine Cahill, Tom Trainor, and the two reviewers for helpful comments. This project was funded by NSF under grant ATM-0926220. We also thank the Flora

Grabowski at the Keith Mather Library in the Geophysical Institute for supporting open access publication of this article.

References

ACRC: Alaska Climate Research Center Climate data for Fairbanks, AK, http://climate.gi.alaska.edu/Climate/Location/TimeSeries/Fairbanks.html, 2011.

ADEC: Alaska Department of Environmental Conservation Supplemental information: $PM_{2.5}$ Designation and Bounadry Recommendations, http://dec.alaska.gov/air/doc/PM25_info.pdf, 2007.

ADEC: Alaska Department of Environmental Conservation Fairbanks non-attainment area boundary comments. Emissions Inventory 2005, http://www.dec.state.ak.us/air/doc/DEC_EPA_Fbks_NA_20oct08.pdf, 2008.

Akagi, S. K., Yokelson, R. J., Wiedinmyer, C., Alvarado, M. J., Reid, J. S., Karl, T., Crounse, J. D., and Wennberg, P. O.: Emission factors for open and domestic biomass burning for use in atmospheric models, Atmos. Chem. Phys., 11, 4039—4072, doi:10.5194/acp-11-4039-2011, 2011.

Anderson, P. S. and Neff, W. D.: Boundary layer physics over snow and ice, Atmos. Chem. Phys., 8, 3563–3582, doi:10.5194/acp-8-3563-2008, 2008.

Anttila, T., Kiendler-Scharr, A., Tillmann, R., and Mentel, T. F.: On the Reactive Uptake of Gaseous Compounds by Organic-Coated Aqueous Aerosols: Theoretical Analysis and Application to the Heterogeneous Hydrolysis of N2O5, The Journal of Physical Chemistry A, 110, 10 435–10 443, doi:10.1021/jp062403c, http://pubs.acs.org/doi/abs/10.1021/jp062403c, pMID: 16942049, 2006.

Apodaca, R., Huff, D., and Simpson, W.: The role of ice in N_2O_5 heterogeneous hydrolysis at high latitudes, Atmos. Chem. Phys, 8, 7451–7463, doi:10.5194/acp-8-7451-2008, 2008.

ARCTAS: Arctic Research of the Composition of the Troposphere by Aircraft and Satellites NASA DC-8 aircraft data, http://www-air.larc.nasa.gov/cgi-bin/arctas-c, 2008.

Ayers, J. D. and Simpson, W. R.: Measurements of N_2O_5 near Fairbanks, Alaska, J. Geophys. Res., 111, D14 309, doi:10.1029/2006JD007070, 2006.

Bertram, T. and Thornton, J.: Toward a general parameterization of N_2O_5 reactivity on aqueous particles: The competing effects of particle liquid water, nitrate and chloride, Atmos. Chem. Phys, 9, 8351–8363, doi:10.5194/acp-9-8351-2009, 2009.

Bertram, T. H., Thornton, J. A., Riedel, T. P., Middlebrook, A. M., Bahreini, R., Bates, T. S., Quinn, P. K., and Coffman, D. J.: Direct observations of N2O5 reactivity on ambient aerosol particles, Geophysical Research Letters, 36, n/a–n/a, doi:10.1029/2009GL040248, http://dx.doi.org/10.1029/2009GL040248, 2009.

Bott, A., Trautmann, T., and Zdunkowski, W.: A numerical model of the cloudtopped planetary boundary layer: Radiation, turbulence and spectral microphysics in marine stratus, Q. J. R. Meteorol. Soc., 122, 635–667, 1996.

Brandt, C. and van Eldik, R.: Transition metal-catalyzed oxidation of sulfur (IV) oxides Atmospheric-relevant processes and mechanisms, Chem. Rev., 95, 119–190, 1995.

Brown, S., Stark, H., Ryerson, T., Williams, E., Nicks, D., Trainer, M., Fehsenfeld, F., and Ravishankara, A.: Nitrogen oxides in the nocturnal boundary layer: Simultaneous in situ measurements of NO_3, N_2O_5, NO_2, NO, and O_3, J. Geophys. Res., 108, 2917, doi:10.1029/2002JD002917, 2003.

Brown, S., Dubé, W., Osthoff, H., Stutz, J., B., R. T., Wollny, A. G., Brock, C. A., Warneke, C., de Gouw, J. A., Atlas, E., Neuman, J. A., Holloway, J. S., Lerner, B. M., Williams, E. J., Kuster, W. C., Goldan, P. D., Angevine, W. M., Trainer, M., Fehsenfeld, F. C., and Ravishankara, A. R.: Vertical profiles in NO_3 and N_2O_5 measured from an aircraft: Results from the NOAA P-3 and surface platforms during the New

England Air Quality Study 2004, J. Geophys. Res., 112, doi:10.1029/2007JD008883, 2007a.

Brown, S. S., Dubé, W. P., Osthoff, H. D., Wolfe, D. E., Angevine, W. M., and Ravishankara, A. R.: High resolution vertical distributions of NO_3 and N_2O_5 through the nocturnal boundary layer, Atmos. Chem. Phys., 7, 139–149, doi:10.5194/acp-7-139-2007, 2007b.

Brown, S. S., Dubé, W. P., Fuchs, H., Ryerson, T. B., Wollny, A. G., Brock, C. A., Bahreini, R., Middlebrook, A. M., Neuman, J. A., Atlas, E., Roberts, J. M., Osthoff, H. D., Trainer, M., Fehsenfeld, F. C., and Ravishankara, A. R.: Reactive uptake coefficients for N2O5 determined from aircraft measurements during the Second Texas Air Quality Study: Comparison to current model parameterizations, Journal of Geophysical Research: Atmospheres, 114, n/a–n/a, doi:10.1029/2008JD011679, http://dx.doi.org/10.1029/2008JD011679, 2009.

Chang, W. L., Bhave, P. V., Brown, S. S., Riemer, N., Stutz, J., and Dabdub, D.: Heterogeneous Atmospheric Chemistry, Ambient Measurements, and Model Calculations of N2O5: A Review, Aerosol Science and Technology, 45, 665–695, doi:10.1080/02786826.2010.551672, http://dx.doi.org/10.1080/02786826.2010.551672, 2011.

Dentener, F. J. and Crutzen, P. J.: Reaction of N_2O_5 on Tropospheric Aerosols: Impact on the Global Distributions of NOx, O_3, and OH, J. Geophys. Res, 98, 7149–7163, 1993.

ESRL: Earth System Research Laboratory, Global Monitoring Division, Surface ozone, in-situ hourly averages, Barrow, AK, http://www.esrl.noaa.gov/gmd/dv/data/index.php?site=brw&category=Ozone&parameter_name=Surface%BOzone, 2011.

Evans, M. J. and Jacob, D. J.: Impact of new laboratory studies of N2O5 hydrolysis on global model budgets of tropospheric nitrogen oxides, ozone, and OH, Geophysical Research Letters, 32, n/a–n/a, doi:10.1029/2005GL022469, http://dx.doi.org/10.1029/2005GL022469, 2005.

Fenn, M., Baron, J., Allen, E., Rueth, H., Nydick, K., Geiser, L., Bowman, W., Sickman, J., Meixner, T., and Johnson, D.: Ecological effects of nitrogen deposition in the western United States,, BioScience, 53, 404–420, 2003.

Finlayson-Pitts, B. and Pitts, J.: Chemistry of the Upper and Lower Atmosphere, Academic Press, 2000.

Fochesatto, J., Collins, R., Yue, J., Cahill, C., and Sassen, K.: Compact eye-safe backscatter lidar for aerosol studies in urban polar environment, vol. 5887, pp. 58 870U–58 870U–9, SPIE, 2005.

Gaston, C. J., Thornton, J. A., and Ng, N. L.: Reactive uptake of N_2O_5 to internally mixed inorganic and organic particles: the role of organic carbon oxidation state and inferred organic phase separations, Atmospheric Chemistry and Physics Discussions, 13, 32 053–32 092, doi:10.5194/acpd-13-32053-2013, http://www.atmos-chem-phys-discuss.net/13/32053/2013/, 2013.

Geyer, A. and Stutz, J.: Vertical profiles of NO_3, N_2O_5, O_3, and NO_x in the nocturnal boundary layer: 2 Model studies on the altitude dependence of composition and chemistry, J. Geophys. Res., 109, D12 307, doi:10.1029/2003JD004211, 2004.

Graedel, T. E. and Keene, W. C.: Tropospheric budget of reactive chlorine, Global Biogeochem. Cycles, 9, 47, doi:10.1029/94GB03103, 1995.

Hanson, D. R. and Ravishankara, A. R.: The Reaction Probabilities of $ClONO_2$ and N_2O_5 on 40 to 75% Sulfuric Acid Solutions, J. Geophys. Res., 96, 17 307–17 314, doi:10.1029/91JD01750, 1991.

Hoffman, M. R. and Boyce, S. D.: Catalytic autooxidation of aqueous sulfur dioxide in relationship to atmo-

spheric systems, Adv. Environ. Sci. Technol., 12, 148–189, 1983.

Huff, D. M., Joyce, P. L., Fochesatto, G. J., and Simpson, W. R.: Deposition of dinitrogen pentoxide, N_2O_5, to the snowpack at high latitudes, Atmos. Chem. and Phys., 11, 4929–4938, doi:10.5194/acp-11-4929-2011, 2011.

Jaenicke, R.: Tropospheric aerosols, chap. Chapter 1: Aerosol-Cloud-Climate Interactions, 1993.

Kramm, G., Dlugi, R., Dollard, G., Foken, T., Mölders, N., Müller, H., Seiler, W., and Sievering, H.: On the dry deposition of ozone and reactive nitrogen species, Atmospheric Environment, 29, 3209 – 3231, doi:10.1016/1352-2310(95)00218-N, 1995.

Landgraf, J. and Crutzen, P.: An Efficient Method for 'On-Line' Calculations of Photolysis and Heating Rates, J. Atmos. Sci., 55, 863 – 878, 1998.

Mentel, T. F., Sohn, M., and Wahner, A.: Nitrate effect in the heterogenous hydrolysis of dinitrogen pentoxide on aqueous aerosols, Phys. Chem. Chem. Phys., 2, 5451–5457, doi:10.1039/A905338G, 1999.

NCDC: National Climate Data Center, Relative humidity from Fairbanks, AK station (PAFA), ftp://ftp.ncdc.noaa.gov/pub/data/asos-fivemin/6401-2009/, 2011.

Nowak, J. B., Neuman, J. A., Bahreini, R., Middlebrook, A. M., Holloway, J. S., McKeen, S. A., Parrish, D. D., Ryerson, T. B., and Trainer, M.: Ammonia sources in the California South Coast Air Basin and their impact on ammonium nitrate formation, Geophysical Research Letters, 39, n/a–n/a, doi:10.1029/2012GL051197, http://dx.doi.org/10.1029/2012GL051197, 2012.

Osthoff, H., Roberts, J., Ravishankara, A., Williams, E., Lerner, B., Sommariva, R., Bates, T., Coffman, D., Quinn, P., Dibb, J., Stark, H., Burkholder, J. B., Talukdar, R. K., Meagher, J., Fehsenfeld, F. C., and Brown, S. S.: High levels of nitryl chloride in the polluted subtropical marine boundary layer,, Nature Geoscience, 1, doi:10.1038/ngeo177, 2008.

Pechtl, S., Lovejoy, E. R., Burkholder, J. B., and von Glasow, R.: Modeling the possible role of iodine oxides in atmospheric new particle formation, 6, 503 – 523, 2006.

Piot, M. and von Glasow, R.: The potential importance of frost flowers, recycling on snow, and open leads for ozone depletion events, Atmos. Chem. Phys., 8, 2437–2467, doi:10.5194/acp-8-2437-2008, 2008.

Riedel, T. P., Bertram, T. H., Ryder, O. S., Liu, S., Day, D. A., Russell, L. M., Gaston, C. J., Prather, K. A., and Thornton, J. A.: Direct N_2O_5 reactivity measurements at a polluted coastal site, Atmospheric Chemistry and Physics, 12, 2959–2968, doi:10.5194/acp-12-2959-2012, http://www.atmos-chem-phys.net/12/2959/2012/, 2012.

Riemer, N., Vogel, H., Vogel, B., Anttila, T., Kiendler-Scharr, A., and Mentel, T. F.: Relative importance of organic coatings for the heterogeneous hydrolysis of N2O5 during summer in Europe, Journal of Geophysical Research: Atmospheres, 114, n/a–n/a, doi:10.1029/2008JD011369, http://dx.doi.org/10.1029/2008JD011369, 2009.

Ryder, O. S., Ault, A. P., Cahill, J. F., Guasco, T. L., Riedel, T. P., Cuadra-Rodriguez, L. A., Gaston, C. J., Fitzgerald, E., Lee, C., Prather, K. A., and Bertram, T. H.: On the Role of Particle Inorganic Mixing State in the Reactive Uptake of N2O5 to Ambient Aerosol Particles, Environmental Science Technology, 48, 1618–1627, doi:10.1021/es4042622, http://pubs.acs.org/doi/abs/10.1021/es4042622, 2014.

Seinfeld, J. H. and Pandis, S. N.: Atmospheric Chemistry and Physics, 2nd ed., 2006.

Sommariva, R. and von Glasow, R.: Multi-phase halogen chemistry in the tropical Atlantic Ocean, Environ.

Sci. Technol., 46, 10 429 – 10 437, 2012.

Sommariva, R., Osthoff, H. D., Brown, S. S., Bates, T. S., Baynard, T., Coffman, D., de Gouw, J. A., Goldan, P. D., Kuster, W. C., Lerner, B. M., Stark, H., Warneke, C., Williams, E. J., Fehsenfeld, F. C., Ravishankara, A. R., and Trainer, M.: Radicals in the marine boundary layer during NEAQS 2004: a model study of daytime and night-time sources and sinks, Atmos. Chem. Phys., 9, 3075–3093, doi:10.5194/acp-9-3075-2009, 2009.

State of Alaska: Measurements of NO_x and SO_2 from downtown Fairbanks, 2008–2009, personal communication with Alaska Department of Environmental Conservations, 2011, 2008.

State of Alaska: Aerosol particle composition from downtown Fairbanks, 2006–2010, personal communication with Alaska Department of Environmental Conservations, 2011.

Thornton, J. A., Kercher, J. P., Riedel, T. P., Wagner, N. L., Cozic, J., Holloway, J. S., Dubé, W. P., Wolfe, G. M., Quinn, P. K., Middlebrook, A. M., Alexander, B., and Brown, S. S.: A large atomic chlorine source inferred from mid-continental reactive nitrogen chemistry, Nature, 464, 271—274, doi:10.1038/nature08905, 2010.

TOMS: Total Ozone Mapping Spectrometer (TOMS). What is the total column ozone over your house?, http://toms.gsfc.nasa.gov/teacher/ozone_overhead_v8.html, 2011.

Van Doren, J., Watson, L., Davidovits, P., Worsnop, D., Zahniser, M., and Kolb, C.: Uptake of N_2O_5 and HNO_3 by aqueous sulfuric acid droplets, J. Phys. Chem., 95, 1684–1689, 1991.

von Glasow, R., Sander, R., Bott, A., and Crutzen, P.: Modeling halogen chemistry in the marine boundary layer 1. Cloud-free MBL, J. Geophys. Res., 107, 4352, doi:10.1029/2001JD000942, 2002.

Wagner, N. L., Riedel, T. P., Young, C. J., Bahreini, R., Brock, C. A., Dubé, W. P., Kim, S., Middlebrook, A. M., Öztürk, F., Roberts, J. M., Russo, R., Sive, B., Swarthout, R., Thornton, J. A., VandenBoer, T. C., Zhou, Y., and Brown, S. S.: N2O5 uptake coefficients and nocturnal NO2 removal rates determined from ambient wintertime measurements, Journal of Geophysical Research: Atmospheres, 118, 9331–9350, doi:10.1002/jgrd.50653, http://dx.doi.org/10.1002/jgrd.50653, 2013.

Wesely, M.: Parameterization of surface resistances to gaseous dry deposition in regional-scale numerical models, Atmospheric Environment, 23, 1293–1304, 1989.

Wesely, M. and Hicks, B.: A review of the current status of knowledge on dry deposition, Atmospheric Environment, 34, 2261–2282, 2000.

Wood, E., Bertram, T., and Wooldridge, P.: Measurements of N_2O_5, NO_2, and O_3 east of the San Francisco Bay, Atmos. Chem. Phys., 5, 483–491, doi:10.5194/acp-5-483-2005, 2005.

Yokelson, R. J., Griffith, D. W. T., and Ward, D. E.: Open-path Fourier transform infrared studies of large-scale laboratory biomass fires, J. Geophys. Res., 101, 21 067–21 080, doi:10.1029/96JD01800, 1996.

Yokelson, R. J., Susott, R., Ward, D. E., Reardon, J., and Griffith, D. W. T.: Emissions from smoldering combustion of biomass measured by open-path Fourier transform infrared spectroscopy, J. Geophys. Res., 102, 18 865–18 877, doi:10.1029/97JD00852, 1997.

Table 1. Emissions of pollutants in the base model case (at end of emissions, $t = 4\,\mathrm{h}$) and observations from downtown Fairbanks. Q1–Q3 refers to first to third quartile range.

Emission Parameter	Base case 5 m, $t = 4\,\mathrm{h}$	Observed Q1–Q3 or average	Reference
NO_x ($\mathrm{nmol\,mol^{-1}}$)	58	31–103	downtown Fairbanks, Nov 2008 (State of Alaska, 2008)
SO_2 ($\mathrm{nmol\,mol^{-1}}$)	12	8.8–20.6	downtown Fairbanks, Nov 2008 (State of Alaska, 2008)
NH_3 ($\mathrm{nmol\,mol^{-1}}$)	1.5	–	no known observations
$PM_{2.5}$ ($\mathrm{\mu g\,m^{-3}}$)	19	19	downtown Fairbanks, Nov 2008 average (ADEC, 2007)
$PM_{2.5}$ SO_4^{2-} (% mass)	0.18 %	0.18 %	downtown Fairbanks, Nov 2008 average (ADEC, 2007)
$PM_{2.5}$ Cl^- (% mass)	0.4 %	0.5 %	downtown Fairbanks, Nov average (State of Alaska, 2011)
$PM_{2.5}$ NH_4^+/SO_4^{2-} ($\mathrm{mol\,mol^{-1}}$)	1.5	1.5–2.4	downtown Fairbanks, annual average (State of Alaska, 2011)

Table 2. Field observations of NO_x from downtown Fairbanks, University of Alaska Fairbanks (UAF), and the Quist Farm as well related model results. A wind speed of $1\,\mathrm{m\,s^{-1}}$ and distance from downtown was used to calculate corresponding model time. Observations at UAF were performed at an elevation 80 m above the valley floor ([1]) and compared to modeled values in layer centered at 75 m ([2]).

	Downtown	UAF	Quist Farm
Distance from downtown (km, direction)	0	5, WNW	20, WSW
Corresponding model time (h)	4	5	8
Modeled NO_x ($\mathrm{nmol\,mol^{-1}}$)	58	24[2]	12
Observed NO_x range ($\mathrm{nmol\,mol^{-1}}$)	1–390	0–100[1]	0–15
Modeled N_2O_5 ($\mathrm{pmol\,mol^{-1}}$)	38	182[2]	412
Observed N_2O_5 range ($\mathrm{pmol\,mol^{-1}}$)	–	0–250[1]	0–80
Reference	State of Alaska (2008)	Ayers and Simpson (2006)	Huff et al. (2011)

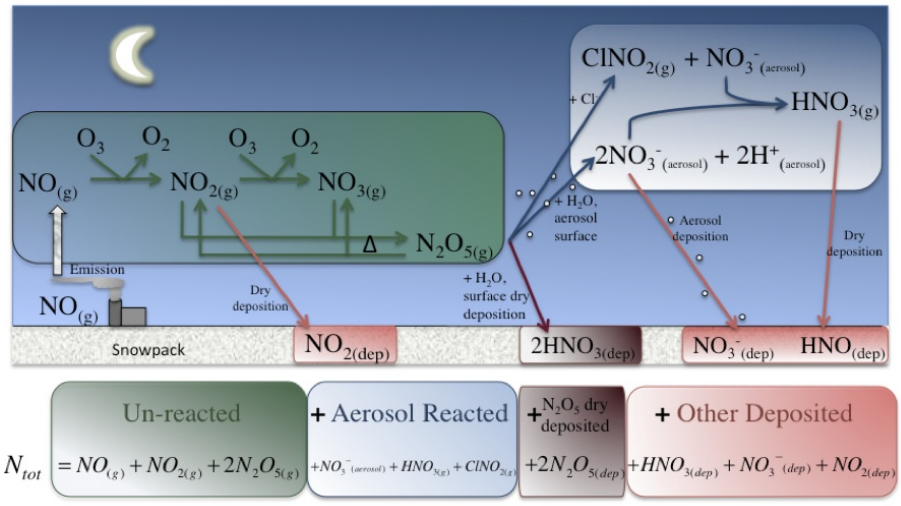

Fig. 1. A nocturnal nitrogen schematic with emphasis on N_2O_5 reactivity. The total nitrogen equation (N_{tot}) is a sum of the total column integrated nitrogen from emitted NO_x, divided into speciation fractions.

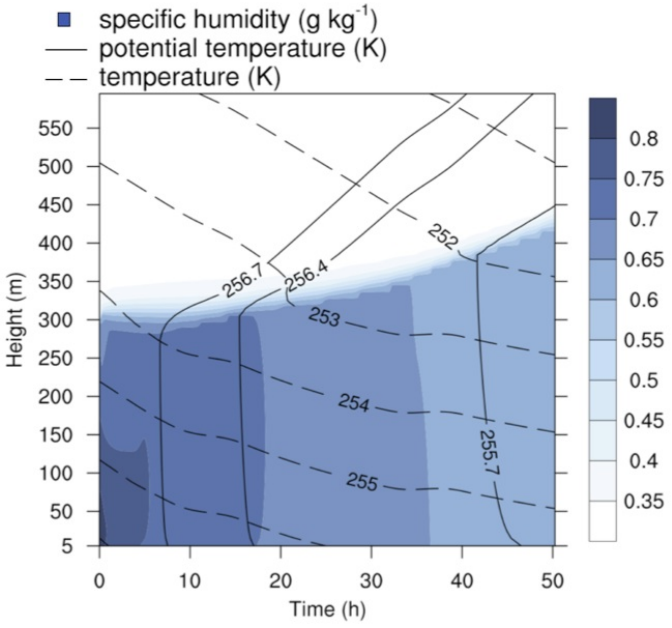

Fig. 2. Modeled meteorological parameters include temperature (dashed contours), potential temperature (solid contours), and specific humidity (blue). The boundary layer height is initialized to be 300 m.

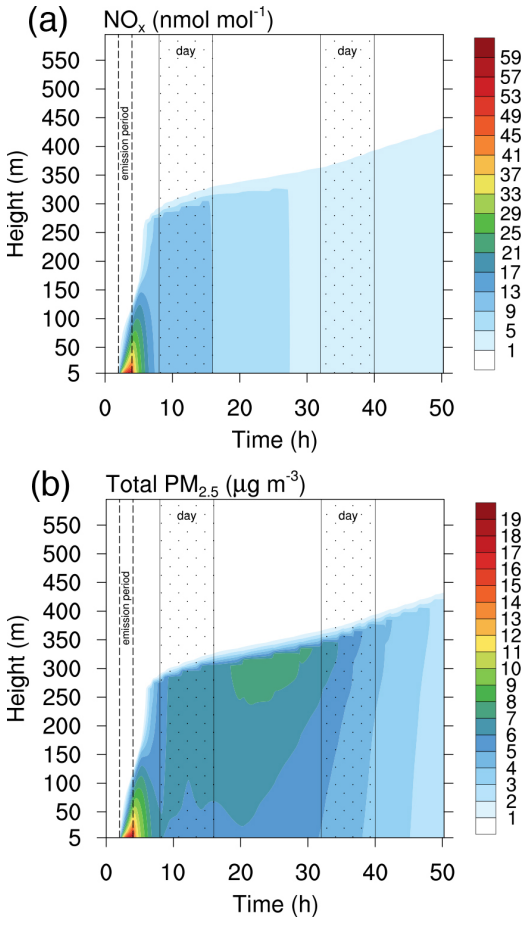

Fig. 3. Modeled evolution of primary emission NO_x and total $PM_{2.5}$ beginning at local midnight. Daytime regions are indicated by the dotted region and the emission period is indicated by the dashed lines. Emitted species dilute throughout the mixed layer. NO_x undergoes chemical loss **(a)** while total $PM_{2.5}$ increases **(b)**, primarily due to formation of particulate nitrate.

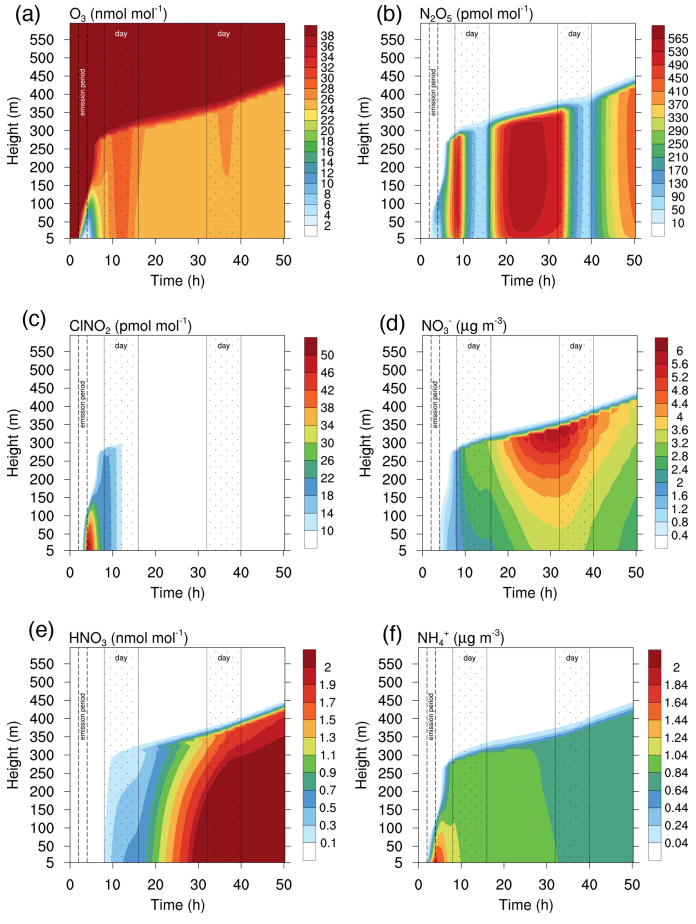

Fig. 4. Contour plots of important gas phase species. Modeled NO_3^- and NH_4^+ are total aerosol mass density (sum of all aerosol particle sizes). Daytime regions are indicated by the dotted region and the emission period is indicated by the dashed lines.

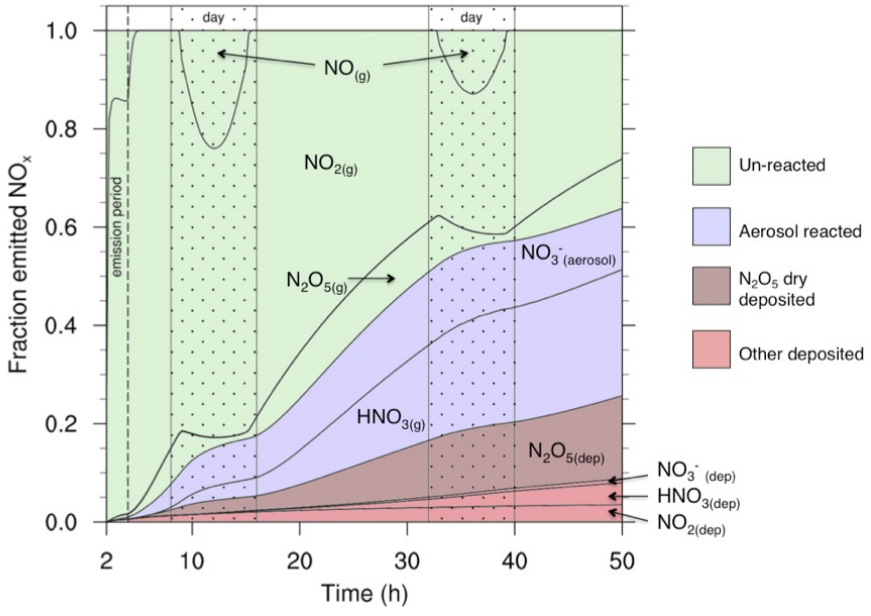

Fig. 5. Speciation diagram of reactive nitrogen species showing column integrated concentrations plus time integrated depositional loss as a function of time. Color categories correspond to Fig. 1.

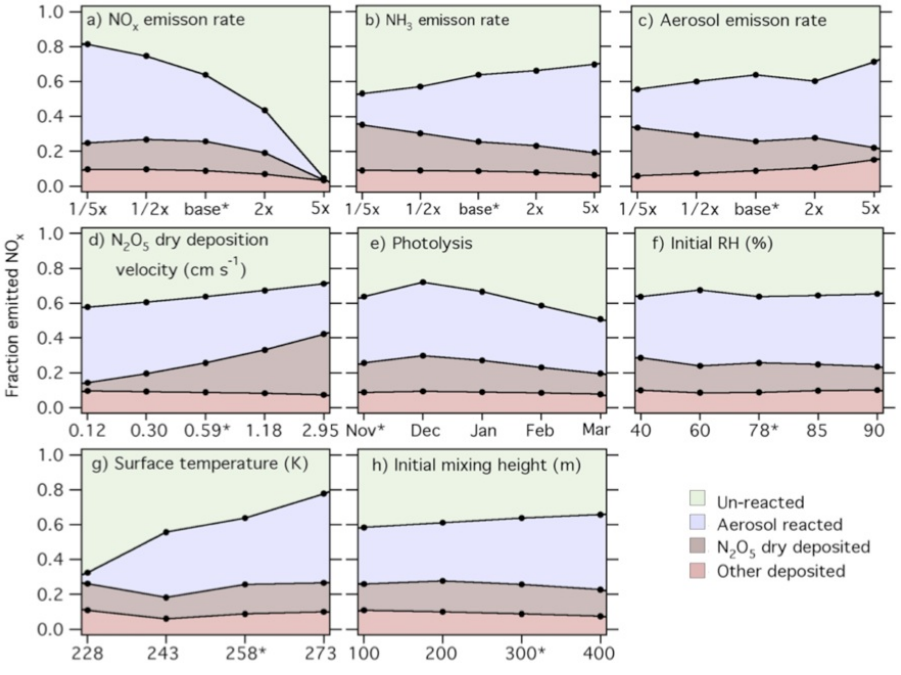

Fig. 6. Sensitivity of the fate of emitted $\mathrm{NO_x}$ to model parameters was investigated by variations of constraints on the base case. Shown are speciation fractions of total column nitrogen emitted as $\mathrm{NO_x}$ at $t = 50\,\mathrm{h}$, corresponding to two days after the emission period begins. Base case runs are marked by an asterisk (*).

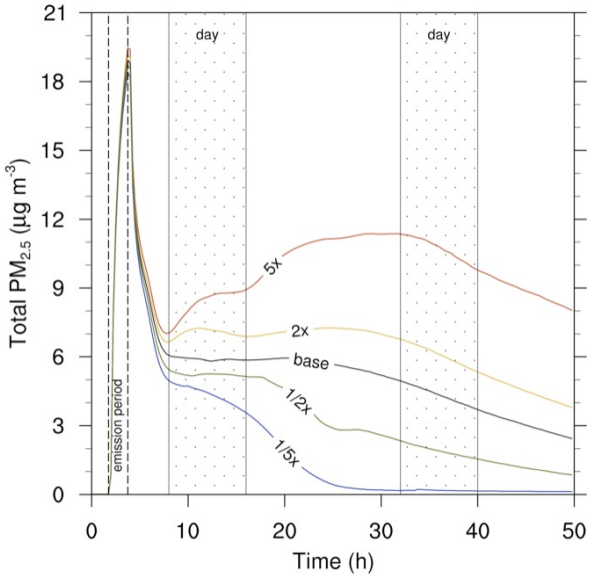

Fig. 7. Secondary formation of ammonium nitrate begins at $t = 8\,\mathrm{h}$ and is controlled in magnitude by $\mathrm{NH_3}$ abundance. The delay of ammonium nitrate formation after emissions end is due to the slowness of nocturnal oxidation caused by ozone titration present during the first night. Pictured above is total $\mathrm{PM_{2.5}}$ for the lowest model layer ($5\,\mathrm{m}$) for each $\mathrm{NH_3}$ sensitivity experiment.